encit 2020

ABCM Associação Brasileira de Engenharia e Ciências Mecânicas

18th Brazilian Congress of Thermal Sciences and Engineering
November 16–20, 2020 (Online)

ENC-2020-0124
REAL-TIME ESTIMATION OF THE AIRSPEED AND THE HEAT TRANSFER COEFFICIENT OF AN AERONAUTICAL PITOT TUBE UNDERGOING ICE ACCRETION

Steve B. Diniz[a]
César C. Pacheco[a]
[a]Engineering School, Fluminense Federal University (UFF), Rua Passo da Pátria, 156, São Domingos, Niterói, RJ, Brazil, 24210-240
Correspondence author email: stdiniz@id.uff.br

Abstract. *This paper presents the use of the Kalman filter technique for real-time estimation of the airspeed and heat transfer coefficient at the tip of an aeronautical Pitot tube undergoing ice accretion. Based on previous works and models available in the literature a new framework is developed for replacing the typical batch estimation process by an approach in which the inverse problem is recasted as a state estimation problem that can be solved using the Kalman filter technique. The forward problem consists of an one dimensional transient heat conduction model used in previous works and a lumped analysis. A Fortran90 algorithm was developed for Kalman filter implementation and a good agreement between reference and estimated airspeed, temperature and convective heat transfer coefficient is observed, thus proving the proposed approach to be robust. The algorithm developed require a low performance computer hardware and can estimate in real-time the sought parameters.*

Keywords: *Kalman Filter, Inverse problem, Ice accretion, Pitot tube, Recursive estimator*

1. NOMENCLATURE

A	cross-sectional area (m^2)	v	airspeed (m/s)
c_p	specific heat capacity ($\mathrm{J\ kg^{-1}\ ^\circ C^{-1}}$)	$\mathbf{v}_i$	vector of noise in the observation model
$\mathbf{F}_i$	state evolution matrix	$\mathbf{w}_i$	vector of noise in the evolution model
g	heat generation density ($\mathrm{W\ m^{-3}}$)	x	coordinate (m)
h	heat transfer coefficient ($\mathrm{W\ m^{-2}\ ^\circ C^{-1}}$)	$\triangle x$	coordinate step (m)
$\mathbf{H}_i$	observation matrix	$\mathbf{x}$	state vector
k	thermal conductivity ($\mathrm{W\ m^{-1}\ ^\circ C^{-1}}$)	$\hat{\mathbf{x}}_i$	posterior estimate of the state vector
$\mathbf{K}_i$	Kalman gain matrix	$\hat{\mathbf{x}}_{i\|i-1}$	prior estimate of the state vector
L	pitot tube length (m)	$\mathbf{y}$	observation vector
n	number of nodal points	***Greek letters***	
p	cross-section perimeter (m)	α	independent term coefficient
$\mathbf{P}_{i\|i-1}$	prior estimation error covariance matrix	β	independent term coefficient
$\mathbf{P}_i$	posterior estimation error covariance matrix	ρ	density ($\mathrm{kg\ m^{-3}}$)
$\mathbf{Q}_i$	evolution noise covariance matrix	ν	kinematic viscosity ($\mathrm{m^2\ s^{-1}}$)
$\mathbf{R}_i$	observation noise covariance matrix	***Superscripts***	
t	time (s)	^	estimate
$\triangle t$	time step (s)	***Subscripts***	
T_{av}	transversally averaged temperature ($^\circ$C)	∞	value at steady-state
T_{aw}	adiabatic wall temperature ($^\circ$C)		

2. INTRODUCTION

The Pitot tube is an instrument that indicates flow speed by using pressure measurements. In aeronautic applications, this instrument provides an indication of the airspeed, thus being an important device for controlling the aerodynamic forces in the airplane structure. In such applications, the Pitot tube can be exposed to extreme flow conditions so that ice accretion can occur in the tip of the Pitot tube, blocking partially or totally the stagnation point and hindering the airspeed measurement. The continuous monitoring of the convective heat transfer coefficient at the tip of the Pitot tube can indicate an ice accretion showing that the airspeed indications may be wrong. During an ice accretion the temperature fields of the

Pitot tube can be estimated and the solution of the ice accretion detection problem consists in solving the inverse problem of heat transfer to obtain the convective heat transfer coefficient based on information regarding the probe temperature.

A major difficulty of most inverse problems analyses is that the required computational efforts typically exceeds the cost of solving the forward problem by orders of magnitude, oftentimes rendering the entire process infeasible. Furthermore, several inverse techniques perform the so-called "batch estimation process" in which all measurements are processed at once. In such situation, one cannot expect to perform any kind of real-time estimation in transient problems, for the history of the sought variable can only be quantified after the final measurement be acquired. However, another set of techniques has been derived for what is known as "recursive estimation", where each new measurement is processed at once (Simon, 2006). In this framework, it has been shown that very low computational times can be achieved, making real-time estimation possible. Such improvements can be found in the literature for heat flux estimation (Pacheco *et al.*, 2014, 2016) and magnetic resonance thermometry (Pacheco *et al.*, 2018, 2020), for example.

In the present work, the proposed inverse problem is solved as a state estimation problem, in a sequential manner by use of the Kalman filter (KF). The KF methodology was implemented in a Fortran90 algorithm to estimate in real-time the convective heat transfer coefficient at the tip of the Pitot tube and airspeed. Airspeed estimation is obtained by using the estimate of the convective heat transfer coefficient at the middle of the Pitot tube, where no ice accretion is expected to occur. Andrade *et al.* (2014) and Souza *et al.* (2016) estimated the same Pitot tube unknowns parameters but these works solved the inverse heat transfer problem using the particle filter methodology, based on Sampling Importance Resampling (SIR) algorithm, that did not allow the real-time monitoring of the Pitot tube parameters due to its high computational cost.

3. MATHEMATICAL FORMULATION

The geometry and physical parameters assumed in this work refer to the PH510 Pitot tube model manufactured by Aero-Instruments, Co, presented in Fig. 1a. The choice of this probe was due to the existence of previous works in the literature that use this probe model and provided comparative data used in this work. The mathematical model assumed in this work was developed by Souza *et al.* (2016). The main part of the Pitot tube is formed by a thin sheet metal (copper at the front and brass at the tail) assumed to be isotropic and the geometry is axisymmetric. The areas where ice accretion is expected, according to Andrade *et al.* (2014), are the stagnation region at the conical tip and the probe support to the airplane structure as can be seen in Fig. 1b.

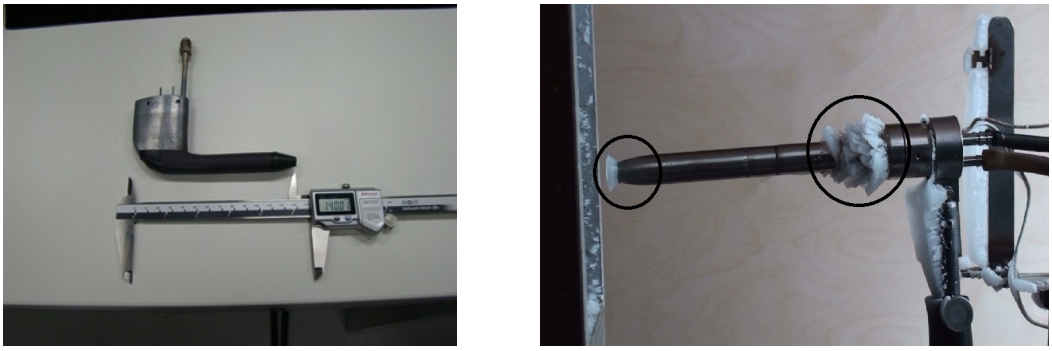

(a) (b)

Figure 1: Design of the Pitot tube: a) PH510 model manufactured by Aero-Instruments, Co. (Souza *et al.*, 2016); b) Areas where ice accretion is expected (highlighted in black). Adapted from Andrade *et al.* (2014).

The main objective of this work is to estimate the convective heat transfer coefficient at the tip of the Pitot tube. This is an important engineering problem because this coefficient changes with the presence of ice and ice accretion in the tip of the Pitot tube hindering the airspeed measurement. The proposed heat conduction model for the forward problem consists of a lumped analysis, whose governing equation is given by Eq. (1):

$$\rho(x)c_p(x)\frac{\partial T_{av}(x,t)}{\partial t} = \frac{1}{A(x)}\frac{\partial}{\partial x}\left[k(x)A(x)\frac{\partial T_{av}(x,t)}{\partial x}\right] - \frac{h(x)p(x)}{A(x)}(T_{av}(x,t) - T_{aw}) + g(x,t), \quad 0 < x < L, \quad t > 0. \tag{1}$$

Associated with Eq. (1), adequate boundary conditions and initial condition are set and given by Eqs. (2a)-(2c):

$$h(x)T_{av}(x,t) - k(x)\frac{\partial T_{av}(x,t)}{\partial x} = h(x)T_{aw}, \quad x = 0, \quad t > 0; \tag{2a}$$

$$\frac{\partial T_{av}(x,t)}{\partial x} = 0, \quad x = L, \quad t > 0; \tag{2b}$$

$$T(x,0) = T_{aw}, \quad 0 \leq x \leq L, \quad t = 0. \tag{2c}$$

The length of the Pitot tube is $L = 0.1596$ m and its internal heat generation term corresponds to the energy provided by an internal electrical resistance (Souza *et al.*, 2016). The explicit finite volume formulation (Versteeg and Malalasekera, 2007), was used for solving Eqs. (1) and (2a)-(2c) and Fig. 2 indicates the parameter curves of the Pitot tube (Andrade *et al.*, 2014). As can be seen the parameters vary along the Pitot tube length (i.e. the x-axis). Furthermore, the exact values for $A, p, k, g, \rho c_p$ and h were not directly available and were extracted graphically from Fig. 2.

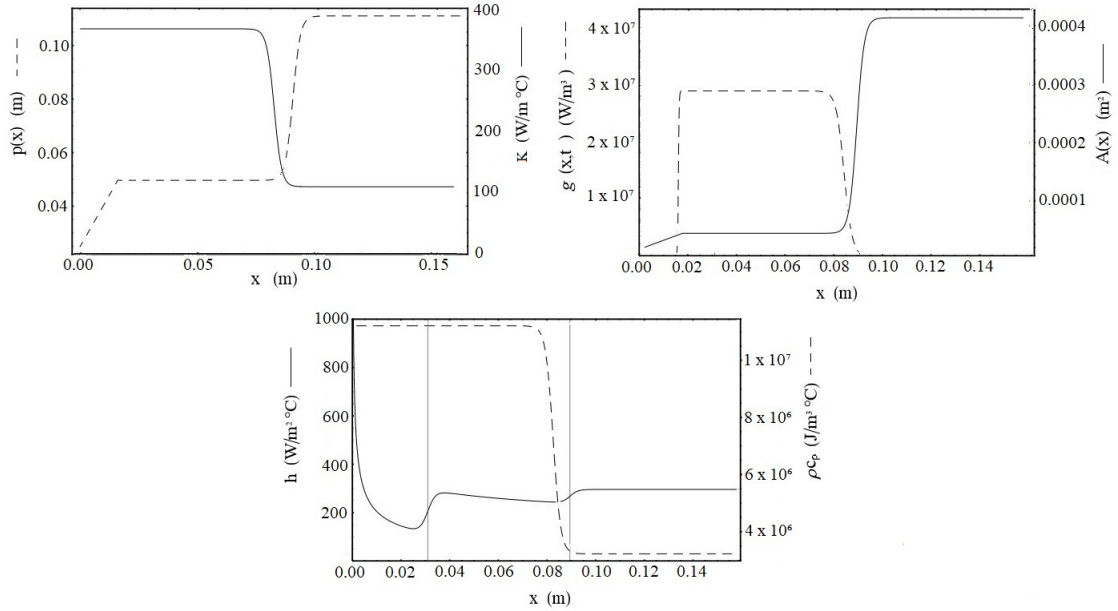

Figure 2: Parameter curves of the Pitot tube. Source: Andrade *et al.* (2014).

A Fortran90 code was developed in order to numerically solve this forward problem and its results were compared with results given by Andrade *et al.* (2014) and Souza *et al.* (2016). The differences between these works is that the latter estimated the surface temperatures at steady-state of the PH510 Pitot tube in a wind tunnel using a free stream velocity of 10 m/s of dry air at 22°C while the former estimated these temperatures using dimensional information of the Airbus Pitot tube and flight conditions of 243.22 m/s airspeed at -52°C. To perform the comparison with Andrade *et al.* (2014) this work used the dimensional data of the Airbus Pitot tube on the mathematical formulation. The developed forward model obtained a very good agreement with the results of the literature as can be seen in Fig. 3 and the small deviations observed in Figs. 3a and 3b are explainable due to the fact that the parameters of the Fig. 2 were extracted graphically. Finally, grid convergence tests were performed in order to assure grid independence.

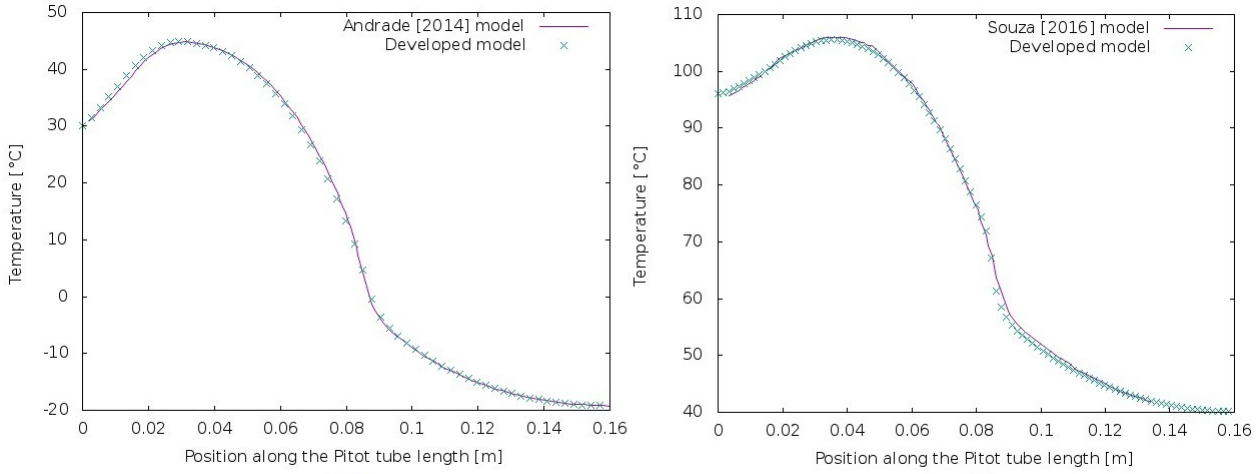

Figure 3: Comparison between temperature profiles of the Pitot tube at steady-state: flight conditions as given by a) Andrade *et al.* (2014); and b) Souza *et al.* (2016).

4. INVERSE PROBLEM

The forward problem given above deals with obtaining the temperature field after establishing values for all the parameters of the model: thermal properties, initial condition, external temperature etc. This includes the convective heat transfer coefficient at the tip of the probe, which is precisely the quantity being sought. Therefore, the solution of the proposed problem calls for an inverse analysis to be performed, which in this work has been done by employing the Kalman Filter (KF). This choice seeks to make possible the real-time estimation of the convective heat transfer coefficients. Being a recursive technique and having a simple structure, the required computational runtime is drastically reduced when using KF, compared with the typical batch estimation process used in previous works in the literature. This technique requires the forward problem equations to be written in the form of the Evolution-Observation Model presented by Eqs. (3a) and (3b).

$$\mathbf{x}_i = \mathbf{F}_i\mathbf{x}_{i-1} + \mathbf{s}_i + \mathbf{w}_{i-1}; \tag{3a}$$

$$\mathbf{y}_i = \mathbf{H}_i\mathbf{x}_i + \mathbf{v}_i. \tag{3b}$$

The KF is a recursive method that operates in two sequential steps named prediction and update (Kalman, 1960; Kaipio and Somersalo, 2006; Simon, 2006). The prediction KF equations are given by Eqs. (4a) and (4b) and the update KF equations are given by Eqs. (4c)-(4e).

$$\hat{\mathbf{x}}_{i|i-1} = \mathbf{F}_i\hat{\mathbf{x}}_{i-1} + \mathbf{s}_i; \tag{4a}$$

$$\mathbf{P}_{i|i-1} = \mathbf{F}_i\mathbf{P}_{i-1}\mathbf{F}_i^T + \mathbf{Q}_i; \tag{4b}$$

$$\mathbf{K}_i = \mathbf{P}_{i|i-1}\mathbf{H}_i^T(\mathbf{H}_i\mathbf{P}_{i|i-1}\mathbf{H}_i^T + \mathbf{R}_i)^{-1}; \tag{4c}$$

$$\hat{\mathbf{x}}_i = \hat{\mathbf{x}}_{i|i-1} + \mathbf{K}_i(\mathbf{y}_i - \mathbf{H}_i\hat{\mathbf{x}}_{i|i-1}); \tag{4d}$$

$$\mathbf{P}_i = (\mathbf{I} - \mathbf{K}_i\mathbf{H}_i)\mathbf{P}_{i|i-1}, \tag{4e}$$

where $\mathbf{w}_i$ and $\mathbf{v}_i$ are zero mean Gaussian noise vectors, with covariance matrices $\mathbf{Q}_i$ and $\mathbf{R}_i$, respectively; $\mathbf{F}_i$ and $\mathbf{H}_i$ are matrices that accounts for the evolution of the state variables and observations, respectively; $\mathbf{x}_i$ is the state vector; $\hat{\mathbf{x}}_{i|i-1}$ is the prior estimate of the state vector; $\hat{\mathbf{x}}_i$ is the posterior estimate of the state vector; $\mathbf{y}_i$ is the measurement vector; $\mathbf{s}_i$ is a vector that group the independent terms, such as non-homogeneities in the boundary conditions; $\mathbf{P}_{i|i-1}$ is the prior estimation error covariance matrix; $\mathbf{P}_i$ is the posterior error covariance matrix and $\mathbf{K}_i$ is the Kalman gain matrix. The

vectors and matrices, for a mesh with n nodal points have the following structures:

$$\hat{\mathbf{x}}_i = (T_{1,i}, T_{2,i}, T_{3,i}, \ldots, T_{n,i}, ht_i, hm_i)_{(n+2)\times 1}; \tag{5a}$$

$$\mathbf{y}_i = (T_{1,i}, T_{2,i}, T_{3,i}, \ldots, T_{n,i})_{n\times 1}; \tag{5b}$$

$$\mathbf{s}_i = (s_1, s_2, s_3, \ldots, s_n, 0, 0)_{(n+2)\times 1}; \tag{5c}$$

$$\mathbf{F} = \begin{bmatrix} (\mathbf{I}_{(n\times n)} + \mathbf{A}_{(n\times n)} \triangle t) & \mathbf{D}_{(n\times 2)} \\ \mathbf{0}_{(2\times n)} & \mathbf{I}_{(2\times 2)} \end{bmatrix}_{(n+2)\times(n+2)}; \tag{5d}$$

$$\mathbf{D} = \begin{bmatrix} \alpha & 0 \\ 0 & 0 \\ \vdots & \vdots \\ 0 & \beta \\ 0 & 0 \\ \vdots & \vdots \\ 0 & 0 \end{bmatrix}_{n\times 2}; \tag{5e}$$

$$\mathbf{H} = \begin{bmatrix} \mathbf{I}_{(n\times n)} & \mathbf{0}_{(n\times 2)} \end{bmatrix}_{n\times(n+2)}; \tag{5f}$$

$$\mathbf{Q} = \begin{bmatrix} \sigma_T^2 \mathbf{I}_{(n\times n)} & \mathbf{0}_{(n\times 2)} \\ \mathbf{0}_{(2\times n)} & \sigma_q^2 \mathbf{I}_{(2\times 2)} \end{bmatrix}_{(n+2)\times(n+2)}; \tag{5g}$$

$$\mathbf{R} = \begin{bmatrix} \sigma_y^2 \mathbf{I}_{(n\times n)} \end{bmatrix}_{n\times n}, \tag{5h}$$

where α and β are coefficients related to the convective heat transfer coefficient at the tip (ht_i) and at the middle (hm_i) of the Pitot tube, respectively. They are mathematically described by Eqs. 6a and 6b. These coefficients are positioned respectively on the first and on the (n/2)-th line of auxiliary matrix $\mathbf{D}$ and x_1 and $x_{n/2}$ are the coordinates of the first and the (n/2)-th nodal points, thus being given by Eqs. (6a) and (6b). The matrix $\mathbf{I}_{(2\times 2)}$ inside the $\mathbf{F}$ matrix is due to the Gaussian random walk model assigned to the convective heat transfer coefficients at the tip and middle of the Pitot tube.

$$\alpha = \frac{A(x_1 - (\triangle x/2)) \triangle t}{A(x_1)\rho(x_1)c_p(x_1) \triangle x} T_{aw}; \tag{6a}$$

$$\beta = \frac{p(x_{n/2}) \triangle t}{A(x_{n/2})\rho(x_1)c_p(x_1)} T_{aw}. \tag{6b}$$

In this work, a set of synthetic measurements was assumed available, obtained from a reference convective heat transfer coefficient profile. Thus, the measurement vector $\mathbf{y}_i$ was simulated from the forward model, later adding Gaussian noise with standard deviation $\sigma_y = 1.5°\text{C}$, according to Eqs. (7a) and (7b). As for the standard deviations of the state variables it was assumed that $\sigma_T = 0.5°\text{C}$ and $\sigma_q = 20.0$ W m^{-2}°C^{-1}.

$$y_i = y_i^{exact} + \sigma_y \omega; \tag{7a}$$

$$\omega \sim N(0, 1). \tag{7b}$$

The profile assigned to the reference heat transfer coefficient at the tip of the Pitot tube is shown in Fig. 4, which comprises of step and linear variations. At this point of this research, there is no particular interest in mimicking realistic profiles for the convective heat transfer, but rather in testing the robustness of the desired algorithm. If such a profile can be efficiently recovered, than one expects to obtain a similar success in more realistic scenarios.

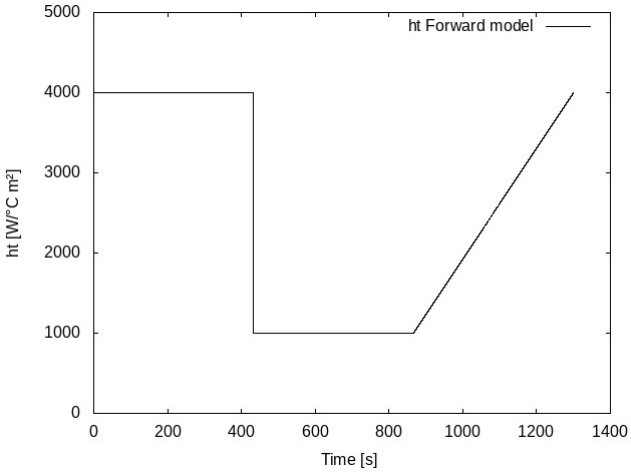

Figure 4: Convective heat transfer coefficient at the tip of the Pitot tube adopted on forward model

As for the airspeed, its estimation was performed by using the formulation for the Nusselt number, given by Eq. (8a) (Özisik *et al.*, 1993). It can be evaluated by using the estimated convective heat transfer coefficient at the middle of the Pitot tube and thermal properties of the air in flight conditions. Rearranging Eq. (8a), the airspeed estimation is given by Eq. (8b):

$$Nu = 0.029 Re^{0.8} Pr^{0.43}; \tag{8a}$$

$$v = \sqrt[0.8]{\left(\frac{hm_i \; L^{0.2} \; \nu^{0.8}}{0.029 \; k \; Pr^{0.43}} \right)}. \tag{8b}$$

The coordinate step is mathematically described by Eq. 9 and from a stability analysis of the Evolution-Observation Model the time step was defined for 10^{-1} seconds. The developed algorithm evaluated the thermal behavior of the Pitot tube in an interval of 1300 seconds after the internal heating system is turned on and tests were performed using a mesh of 60 nodal points.

$$\triangle x = \frac{L}{n} \tag{9}$$

5. RESULTS

5.1 Temperature along the Pitot tube

Figure 5 shows the temperature curves in the Pitot tube at 400 and 800 seconds. As can be seen the KF estimation has a fast convergence and as expected the decrease in the convective heat transfer coefficient, indicated in Fig. 4, increases the temperature at the tip of the Pitot tube. A very good agreement between exact, simulated and estimated values is achieved, which indicates that the KF correctly represented the dynamics of the physical model. Furthermore, Fig. 6 shows the results obtained by use of the KF at steady-state, which takes place around $t = 1300$ s. A plot of the residuals is also shown here, where one can observe that they oscillate around zero. Also, these oscillations take place with magnitude of the same order of the standard deviation of the simulated measurements, thus providing additional evidence that the KF successfully addressed the given inverse problem. This behavior of the residuals is observed throughout the whole numerical experiment and has been omitted for the remaining time steps for the sake of brevity.

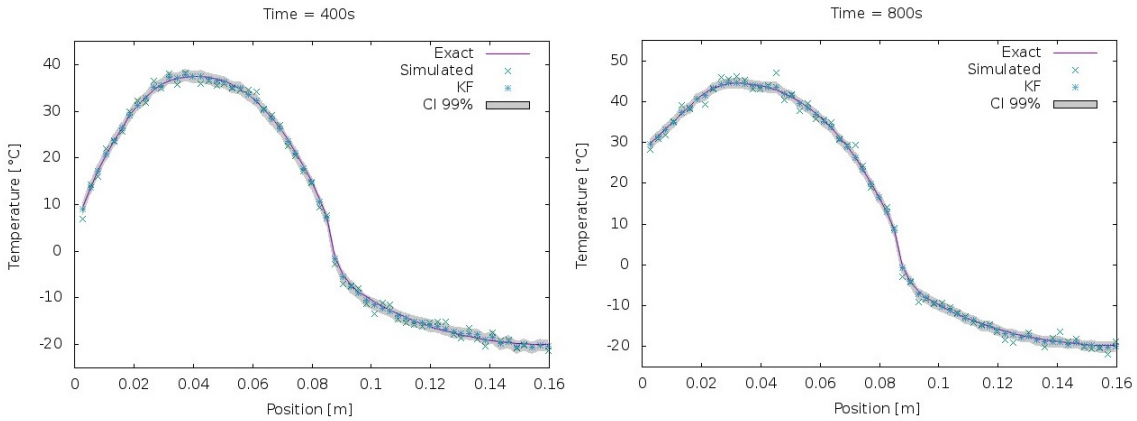

Figure 5: Temperature along the Pitot tube for 400 and 800 seconds after start simulation.

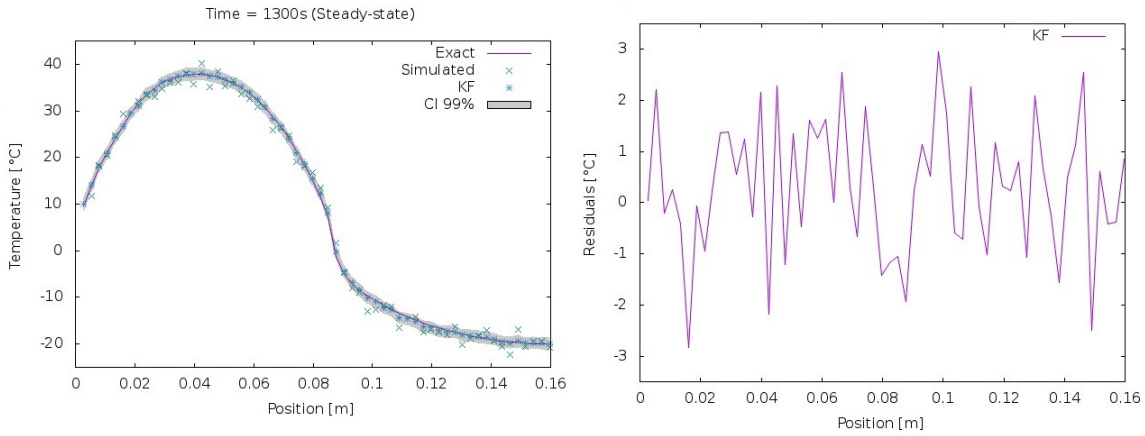

Figure 6: Temperature along the Pitot tube at steady-state (left) and their respective residuals (right).

5.2 Temperature at the tip of the Pitot tube

Figure 7 shows the temperature at the tip of the Pitot tube and their respective residuals, versus time. As can be seen, once again the residuals oscillate around zero, with magnitude of the same order of the standard deviation of the simulated measurements. A small exception occurs at the beginning of the simulation, due to uncertainties in the initial conditions and large gradients in temperature at this point. Nevertheless, a very good agreement is present between exact and reference values. It also bears pointing out that the estimated temperature values are accompanied by their 99% confidence intervals, which completely encapsulates the exact values.

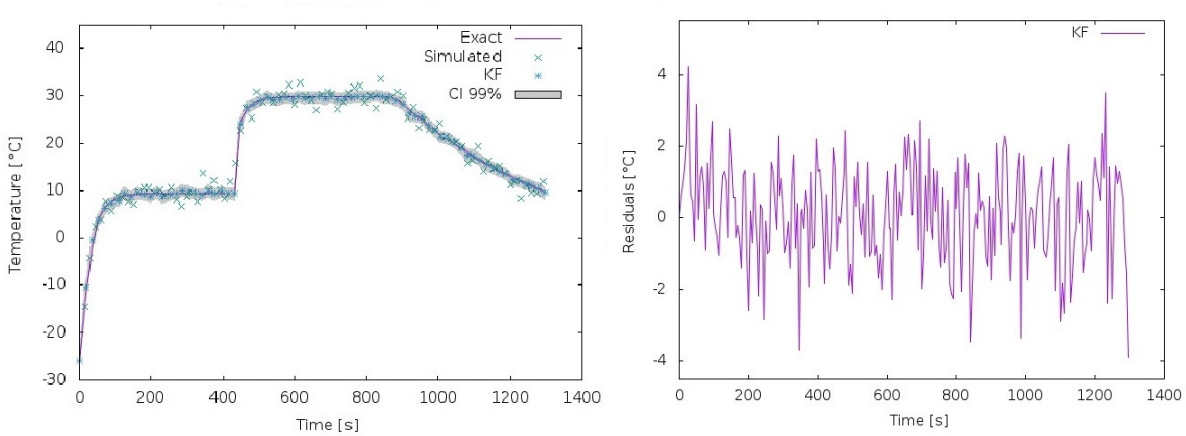

Figure 7: Temperature at the tip of the Pitot tube as a function of time (left) and their respective residuals (right).

5.3 Convective heat transfer coefficient at the tip of the Pitot tube

Figure 8 shows the convective heat transfer coefficient curve at the tip of the Pitot tube estimated by the KF. A very good agreement with forward model results is observed. The KF presented a fast convergence and estimated very well the exact values. As can be seen the KF estimation lose accuracy at moments when the convective coefficient varies very sharply. Nevertheless, it goes back on track of the exact values fast enough. This provides evidence that this algorithm might adequately deal with sudden changes in the convective heat transfer coefficient, which can happen in a situation of ice accretion, for example. A plot of the estimation errors is also present, where it can be seen that very small errors are present, with the sole exception of the abrupt change mentioned above.

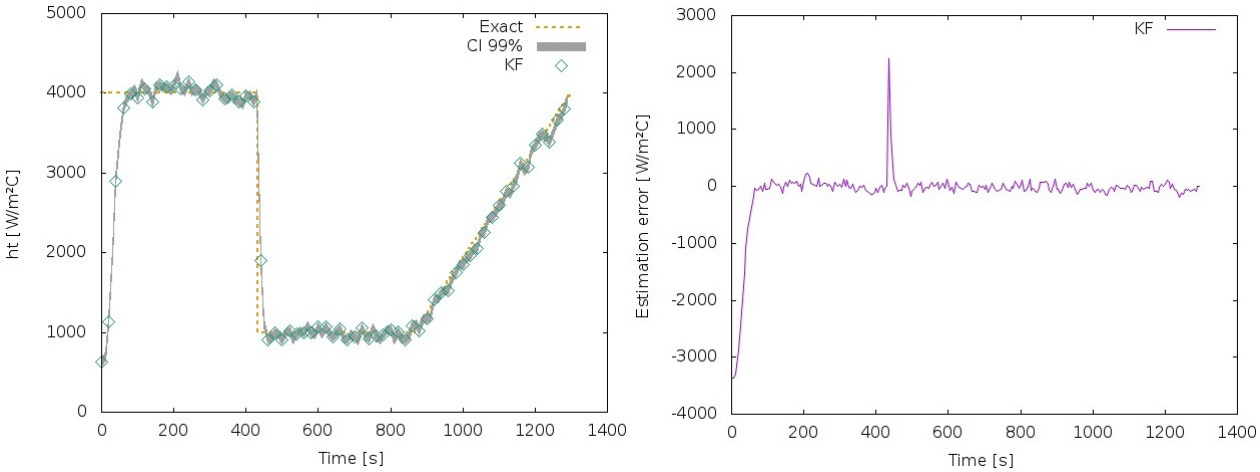

Figure 8: Convective heat transfer coefficient at the tip of the Pitot tube (left) and their respective estimation errors (right).

5.4 Estimated airspeed

The airspeed was estimated using the KF estimation of the convective heat transfer coefficient at the middle of the Pitot tube, thermal properties of the air in flight conditions and Eq. (8b). These calculations yielded an estimate between 250.09 and 250.61 m/s for the airspeed, which presents a deviation between 2.8% and 3% from the exact value of 243.22 m/s. This means that, although not being the main objective of this work, the proposed framework also allows for obtaining a good estimate of the airspeed, which would be extremely helpful in a scenario where the standard measurement methods are somewhat hindered.

5.5 Computational costs

This work employed an old laptop equipped with Intel Core 2 Duo T6500 processor, 4 GB of DDR2 RAM memory and Linux Lubuntu 32 bits operational system and tests were performed using a mesh of 60 nodal points. The KF methodology used in this work can acquire 1300 seconds of data information requiring a solution run time of 77 seconds. This is a very important result, because it means that the recursive estimation provided by the KF can be performed at real-time, which is absolutely paramount for this particular problem. Table 1 presents a brief performance comparison between the Kalman filter and the particle filter (SIR algorithm) for solving the inverse heat transfer problem in the Pitot tube.

Table 1: Solution methodology comparison.

Work	Inverse Problem Solution Methodology	Minimal solution run time	Real-time monitoring
Present work	Kalman Filter	77 seconds	Yes
Andrade *et al.* (2014)	Particle filter - SIR	10800 seconds	No

6. CONCLUSIONS

Considering the proposed conditions, the Kalman Filter presented excellent results and could be used to monitor in real-time the ice accretion in the Pitot tube and airspeed estimation for this condition. The developed model could detect the variations proposed in convective heat transfer coefficient at the tip of the Pitot tube with enough accuracy for detect an ice accretion. The computational hardware necessities are easiest reached with low costs and the code run faster than real-time monitoring.

7. REFERENCES

Andrade, G.J., Orlande, H.R. and Cotta, R.M., 2014. "Use of particle filters to estimate relative air speed in a pitot tube". In *ICHMT Digital Library Online*. Begel House Inc.

Kaipio, J. and Somersalo, E., 2006. *Statistical and computational inverse problems*, Vol. 160. Springer Science & Business Media.

Kalman, R.E., 1960. "A new approach to linear filtering and prediction problems". *Transactions of the ASME–Journal of Basic Engineering*, Vol. 82, No. Series D, p. 35–45.

Özisik, M.N., Özısık, M.N. and Özısık, M.N., 1993. *Heat conduction*. John Wiley & Sons.

Pacheco, C.C., Orlande, H.R.B., Colaço, M.J. and Dulikravich, G.S., 2016. "Real-time identification of a high-magnitude boundary heat flux on a plate". *Inverse Problems in Science and Engineering*, Vol. 24, No. 9, pp. 1661–1679.

Pacheco, C.C., Orlande, H.R.B., Colaço, M.J. and Dulikravich, G.S., 2018. "State estimation problems in prf-shift magnetic resonance thermometry". *International Journal of Numerical Methods for Heat & Fluid Flow*, Vol. 28, pp. 6–8.

Pacheco, C.C., Orlande, H.R.B., Colaço, M.J. and Dulikravich, G.S., 2020. "Real-time temperature estimation with enhanced spatial resolution during mr-guided hyperthermia therapy". *Numerical Heat Transfer Part A: Applications*, Vol. 77, pp. 782–806.

Pacheco, C., Orlande, H., Colaço, M. *et al.*, 2014. "Identification of a position and time dependent heat flux using the kalman filter and improved lumped analysis in heat conduction". In *5th International Conference on Computational Methods. Cambridge, MA*.

Simon, D., 2006. *Optimal state estimation: Kalman, H infinity, and nonlinear approaches*. John Wiley & Sons.

Souza, J., Lisbôa, K.M., Allahyarzadeh, A., de Andrade, G., Loureiro, J.B.R., Naveira-Cotta, C.P., Freire, A.S., Orlande, H.R.B., Silva, G.A.L.d. and Cotta, R.M., 2016. "Thermal analysis of anti-icing systems in aeronautical velocity sensors and structures". *Journal of the Brazilian Society of Mechanical Sciences and Engineering*, Vol. 38, No. 5, pp. 1489–1509.

Versteeg, H.K. and Malalasekera, W., 2007. *An introduction to computational fluid dynamics: the finite volume method*. Pearson education.

8. RESPONSIBILITY NOTICE

The authors are solely responsible for the printed material included in this paper.